Chemistry–A European Journal
Research Article
doi.org/10.1002/chem.202104502
Chemistry Europe
European Chemical Societies Publishing
www.chemeurj.org

Control of Crystallinity of Vinylene-Linked Two-Dimensional Conjugated Polymers by Rational Monomer Design

Dominik L. Pastoetter,[a, b] Yannan Liu,[a] Matthew A. Addicoat,[c] Silvia Paasch,[d] Arezoo Dianat,[e] David Bodesheim,[e] Albrecht L. Waentig,[a] Shunqi Xu,[a, b] Mino Borrelli,[a] Alexander Croy,[f] Marcus Richter,[a] Eike Brunner,[d] Gianaurelio Cuniberti,[e] and Xinliang Feng*[a, b]

Abstract: The interest in two-dimensional conjugated polymers (2D CPs) has increased significantly in recent years. In particular, vinylene-linked 2D CPs with fully in-plane sp^2-carbon-conjugated structures, high thermal and chemical stability, have become the focus of attention. Although the Horner-Wadsworth-Emmons (HWE) reaction has been recently demonstrated in synthesizing vinylene-linked 2D CPs, it remains largely unexplored due to the challenge in synthesis. In this work, we reveal the control of crystallinity of 2D CPs during the solvothermal synthesis of 2D-poly(phenylene-quinoxaline-vinylene)s (2D-PPQVs) and 2D-poly(phenylene-vinylene)s through the HWE polycondensation. The employment of fluorinated phosphonates and rigid aldehyde building blocks is demonstrated as crucial factors in enhancing the crystallinity of the obtained 2D CPs. Density functional theory (DFT) calculations reveal the critical role of the fluorinated phosphonate in enhancing the reversibility of the (semi)reversible C–C single bond formation.

[a] *D. L. Pastoetter, Dr. Y. Liu, A. L. Waentig, Dr. S. Xu, M. Borrelli, Dr. M. Richter, Prof. Dr. X. Feng*
Chair of Molecular Functional Materials, Center for Advancing Electronics Dresden (cfaed) and Faculty of Chemistry and Food Chemistry
Technische Universität Dresden
01062 Dresden (Germany)
E-mail: xinliang.feng@tu-dresden.de

[b] *D. L. Pastoetter, Dr. S. Xu, Prof. Dr. X. Feng*
Department of Synthetic Materials and Functional Devices
Max-Planck Institute of Microstructure Physics
06120 Halle (Germany)

[c] *Dr. M. A. Addicoat*
School of Science and Technology
Nottingham Trent University Clifton Lane
Nottingham, NG118NS (United Kingdom)

[d] *Dr. S. Paasch, Prof. Dr. E. Brunner*
Chair of Bioanalytical Chemistry, Faculty of Chemistry and Food Chemistry
Technische Universität Dresden
01062 Dresden (Germany)

[e] *Dr. A. Dianat, D. Bodesheim, Prof. Dr. G. Cuniberti*
Chair of Material Science and Nanotechnology, Faculty of Mechanical Science and Engineering
Technische Universität Dresden
01062 Dresden (Germany)

[f] *Dr. A. Croy*
Chair of Theoretical Chemistry
Institute of Physical Chemistry
Friedrich Schiller University Jena
07737 Jena (Germany)

Supporting information for this article is available on the WWW under https://doi.org/10.1002/chem.202104502

Introduction

While linear (1D) conjugated polymers (CPs) have been extensively studied in the past decades due to their intrinsic semiconducting behavior,[1] the dimensional increase to two-dimensional (2D) CPs remained unexplored for decades. Since the discovery of graphene, with its semimetallic behavior, zero bandgap, and high charge carrier mobility,[2–4] the bottom-up synthesis of 2D CPs has become appealing for polymer and materials scientists. In particular, imine-linked (C=N) 2D covalent organic frameworks (2D COFs),[5–8] which can also be regarded as π-conjugated 2D CPs, have gained considerable interest in recent years. Nevertheless, the polarization of the carbon-nitrogen bond in the above-mentioned C=N linkage cannot promote efficient conjugation through the 2D backbone.[9] For this reason, recent attention has been focused on carbon-carbon conjugated 2D CPs due to their enhanced π-conjugation over the sp^2-carbon frameworks and high stability compared to the imine-linked 2D COFs. Thus, 2016 marks the ascent of vinylene-linked 2D CPs by employing the Knoevenagel polycondensation.[10] The dimensional increase from linear conjugated polymers to 2D CPs is of particular interest due to the faster-evolving bandgaps[11] and enhanced chemical and physical properties, including chemical and thermal stabilities, and increased charge carrier transport compared to their linear counterparts.[12–16]

Due to the atomically precise integration of (functional) building blocks into ordered and porous sp^2-carbon-conjugated structures with π-delocalization in two dimensions, vinylene-linked 2D CPs have been demonstrated as an efficient light emitter,[17,18] artificial photosystem I,[19] in catalysis,[20,21]

sensors,[22] energy storage,[23,24] and conversion.[25,26] Previously, the Knoevenagel[10,16,18,23,25,27] and other aldol-type polycondensations[20,24,28,29] have been employed for the synthesis of crystalline (cyano)-vinylene-linked 2D CPs. Very recently, we firstly reported the Horner-Wadsworth-Emmons (HWE) reaction as an effective method to synthesize vinylene-linked 2D CPs.[30] The HWE reaction is a well-known olefination reaction using phosphonates and aldehydes (or ketones), defined by a high (*E*)-selectivity under mild conditions[31] and has been early utilized to synthesize linear poly(*p*-phenylene vinylenes) (PPVs).[32–35]

In this work, we elucidate the control of crystallinity during the solvothermal synthesis of 2D-poly(phenylene-quinoxaline-vinylene)s (2D-PPQVs) and 2D-poly(phenylene-vinylene)s (2D-PPVs) through the HWE reaction by rational monomer design. Thereby, we utilize electron-poor fluorinated phosphonates and rigid aldehyde building blocks. In detail, we compare the HWE polycondensations of tetraethyl (1,4-phenylenebis(methylene))bis(phosphonate) (**1**) or ((perfluoro-1,4-phenylene)bis(methylene))bis(phosphonate) (**2**) with 1,3,5-tris(4-formyl-phenyl) benzene (TFPB, **5**), 2,4,6-tris(4-formylphenyl)-1,3,5-triazine (TFPT, **6**), or 2,3,8,9,14,15-hexa(4-formylphenyl)diquinoxalino[2,3-*a*:2′,3′-*c*]phenazine (HATN-6CHO, **7**). Notably, the combination of HATN-6CHO (**7**) or TFPT (**6**) together with the fluorinated phosphonate **2** leads to the successful synthesis of layered 2D CPs (**2D-F-PPV2** and **2D-F-PPQV1**) with good crystallinity. The unique layered crystalline structures of the achieved **2D-F-PPV2** and **2D-F-PPQV1** are evaluated using powder X-ray diffraction (PXRD), nitrogen physisorption measurements, and high-resolution transmission electron microscopy (HR-TEM) analysis. The chemical compositions are investigated by infrared spectroscopy (IR) and ^{13}C solid-state nuclear magnetic resonance spectroscopy (^{13}C-ssNMR). Furthermore, density functional theory (DFT) simulations provide insights into the crucial role of the fluorinated phosphonates for the reversibility of the initial C–C single bond formation and the promoted reactivity during the synthesis of the novel vinylene-linked 2D CPs using the HWE polycondensation.

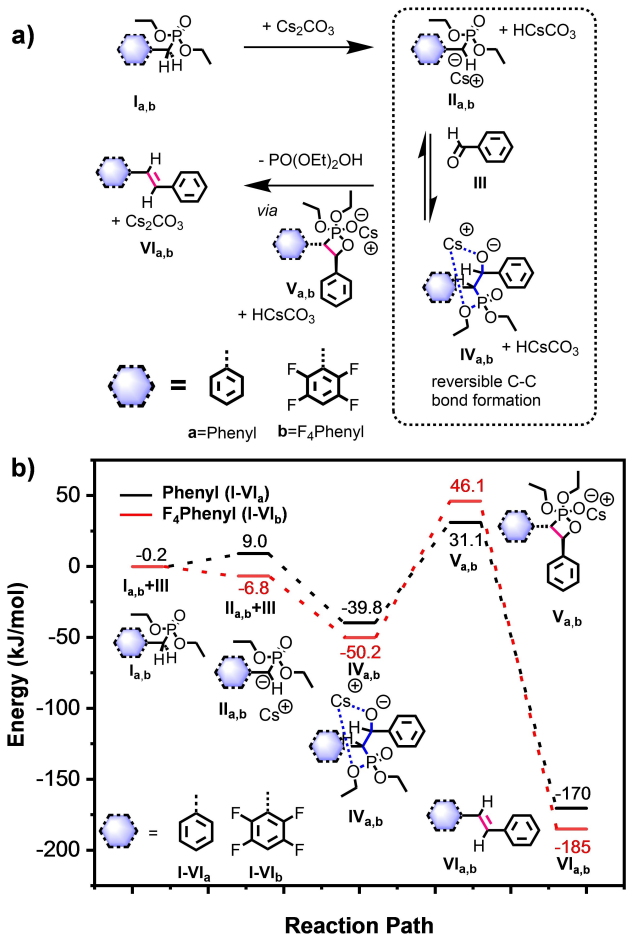

Figure 1. a) Proposed mechanism of the Horner-Wadsworth-Emmons reaction with Cs_2CO_3 as the base. b) Energy profiles at the different stages ($I_{a,b}$–$VI_{a,b}$), calculated in kJ/mol by using the density functional theory (DFT) method, describing the proposed reaction mechanism.

Results and Discussion

To understand the influence of the electronic structure of the phosphonate monomer during the HWE reaction, we compared the model reactions of electron-rich phenyl-phosphonate (I_a) or electron-poor fluorinated phenyl-phosphonate (I_b) with benzaldehyde (**III**) and Cs_2CO_3 as a base. Firstly, we employed DFT calculations in the gas phase to investigate the HWE mechanism displayed in Figure 1a. Based on the DFT calculations (Figure 1b), we draw the following conclusions: i) The electron-poor phosphonate stabilizes the carbanion formation (II_a+**III**: 9.0 kJ/mol, II_b+**III**: −6.8 kJ/mol), leading to an eased deprotonation and C–C single bond formation (IV_a: −39.8 kJ/mol, IV_b: −50.2 kJ/mol); ii) The formation of the oxaphosphetane (V_a: 31.1 kJ/mol, V_b: 46.1 kJ/mol) is destabilized by the electron-poor fluorinated moiety, indicating a higher energy barrier for the formation of the *trans*-vinylene VI_b thus increasing the reversibility of the C–C single bond formation; iii) Moreover, the fluorinated AB model compound VI_b (−185 kJ/mol) is more thermodynamically favored than the non-fluorinated VI_a (−170 kJ/mol) model compound. The same trend can be also observed for electron-poor pyrazine and benzothiadiazole phosphonates for the HWE reaction (Supporting Information, Figure S11). To obtain insights into the reaction speed of the HWE reaction, time-dependent ^1H NMR measurements were studied (Supporting Information, Figure S10). Applied ^1H NMR studies of the reaction of phosphonate **1** or **2** with benzaldehyde (Cs_2CO_3, mesitylene (Mes)/*N*,*N*-dimethylacetamide (DMAc) (1:1), 120 °C) revealed a higher reaction speed for the deprotonation of the fluorinated phosphonate **2**. Time-dependent NMR measurements after 5, 30, 60, 120, and 1200 min reaction time show an almost quantitative conversion/deprotonation of fluorinated phosphonate **2** after 30 min, while phosphonate **1** remains incompletely converted after 20 h. Those findings are congruent to the above DFT calculations and reports in the literature.[36] Nevertheless, despite the difference in reactivity, the isolated yields of 1,4-di((*E*)-styryl)benzene (**3**,

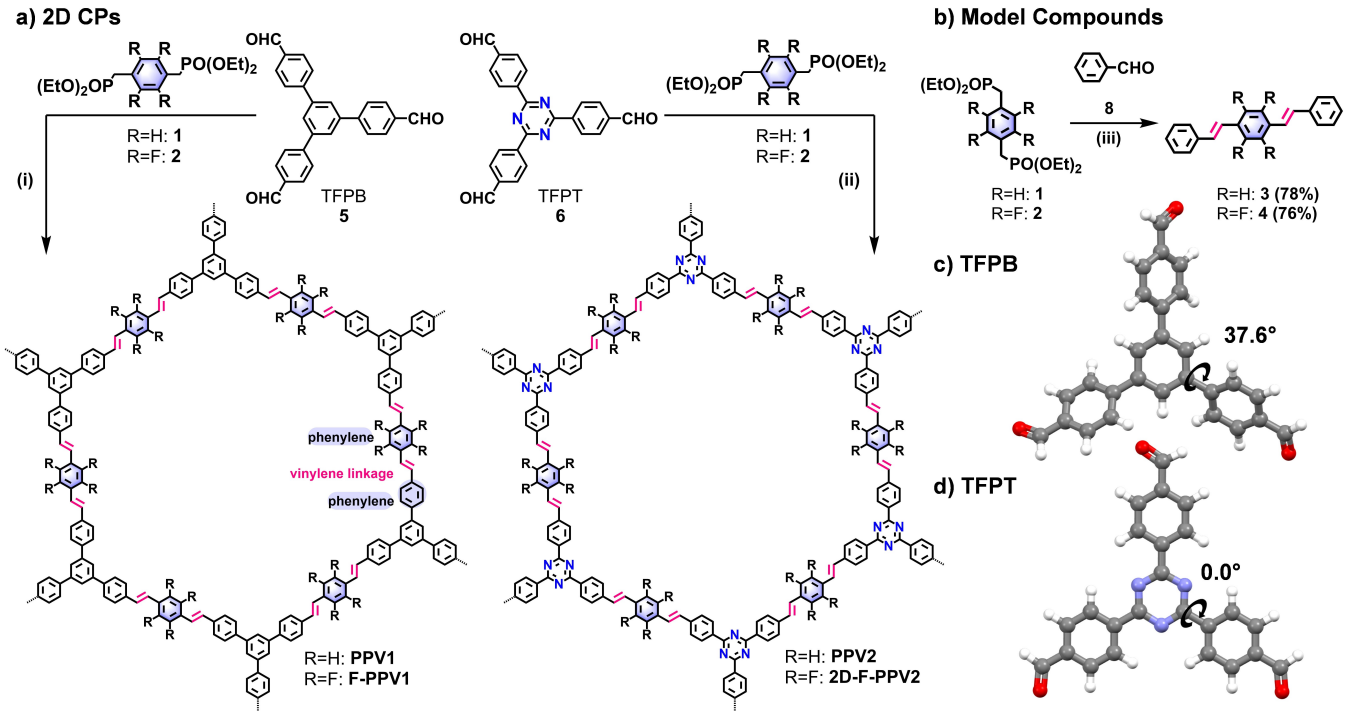

Figure 2. a) Solvothermal synthesis of layered 2D-poly(phenylene-vinylene)s (2D-PPVs) via the Horner-Wadsworth-Emmons polycondensation: In a glass ampule aldehyde (**5** or **6**) (25.4 μmol, 1.0 equiv.), phosphonate (**1** or **2**) (38.1 μmol, 1.5 equiv.), Cs_2CO_3 (27.3 mg, 83.9 μmol, 3.3 equiv.) and 0.8 mL DMAc + o-DCB (1 : 3) was added. After three freeze pump thaw cycles, the tube was sealed under vacuum and then heated to 120 °C for 72 h. b) Synthesis of A_1B_2-type model compounds 1,4-di((*E*)-styryl)benzene (**3**) and ((1*E*,1′*E*)-(perfluoro-1,4-phenylene)bis(ethene-2,1-diyl))dibenzene (**4**): benzaldehyde (**8**) (100 mg, 942 μmol, 4.0 equiv.), phosphonate (**1** or **2**) (236 μmol, 1.0 equiv.), and Cs_2CO_3 (230 mg, 0.706 mmol, 3.0 equiv.) were suspended in 1 mL DMAc + mesitylene (Mes) (1 : 1) under nitrogen and heated at 120 °C for 72 h; Optimized structures (B3LYP 6–31G) of c) TFPB and d) TFPT (C: gray, N: blue, O: red and H: white).

78 %) and ((1*E*,1′*E*)-(perfluoro-1,4-phenylene)bis(ethene-2,1-diyl))dibenzene (**4**, 76 %) are comparable for the respective model compounds (Figure 2b). Thereby, the improved understanding of the model reactions of phosphonates can be beneficial for the synthesis of novel 2D conjugated polymers with improved crystallinity using the semi-reversible HWE reaction.

Next, we compare the A_3B_2-type polycondensations of 1,3,5-tris(4-formyl-phenyl) benzene (TFPB, **5**) or 2,4,6-tris(4-formyl-phenyl)-1,3,5-triazine (TFPT, **6**) as aldehyde monomer together with **1** or **2** as phosphonate building blocks and Cs_2CO_3 as a base in a mixture of DMAc and *o*-dichlorobenzene (*o*-DCB) (1 : 3) at 120 °C (Figure 2a).

For the applied monomer combinations, PXRD data (Figure 3a) reveals the formation of the crystalline fluorinated polymer **2D-F-PPV2** (**2** + **6**, yield ca. 70 %). In contrast, the other monomer combinations **1** + **5** (**PPV1**), **2** + **5** (**F-PPV1**), and **1** + **6** (**PPV2**) only resulted in amorphous polymers (Figure 3b). The amorphous polymers are classified as PPVs, whereas the crystalline polymers are classified as 2D-PPVs. These findings reveal that the employment of electron-poor phosphonate **2** and aldehyde monomers with increased rigidity and decreased conformational degrees of freedom can outweigh low reversibility of the bond formation: TFPT (**6**) shows a planar structure (0.0°) of the triazine core with its attached phenyl rings (Figure 2d), while the external phenyl rings (37.6°) in TFPB (**5**)

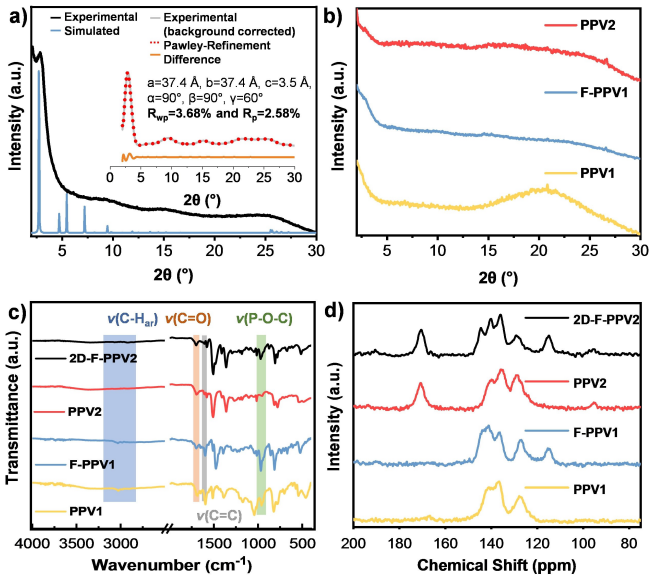

Figure 3. a) PXRD data of **2D-F-PPV2**: Experimental (black) and simulated PXRD with AA stacking (blue), and the background-corrected PXRD shown in the inset (background-corrected experimental data (grey), Pawley-Refinement (red), difference plot (orange)); b) PXRD data of **PPV1** (yellow), **F-PPV1** (blue), and **PPV2** (red); c) IR spectra and d) ^{13}C-ssNMR spectra of **PPV1** (yellow), **F-PPV1** (blue), **PPV2** (red), and **2D-F-PPV2** (black).

are rather twisted (Figure 2c). The layered crystalline structure of **2D-F-PPV2** was manifested by experimental and simulated PXRD patterns (Figure 3a). For **2D-F-PPV2**, a reflex at 2.8° can be assigned to the (100) plane. Density-Functional Tight-Binding (DFTB$^+$ 19.1)[37] was used to optimize the monolayer structures of **2D-F-PPV2** using the Self-Consistent-Charge (SCC-DFTB) method, including Lennard-Jones dispersion. Carbon, nitrogen, oxygen, and hydrogen atoms are described using the mio-0-1 parameter set.[38] The optimized monolayer, AA (eclipsed), AB (staggered), and slipped-AA structures are generated for **2D-F-PPV2**. Optimized interlayer distances, relevant energies, bandgaps, unit cell parameters, HOMO, LUMO, and Fermi level of different stacking modes of **2D-F-PPV2** can be found in the Supporting Information. Pawley refinement of **2D-F-PPV2** was conducted with Accelrys's Materials Studio 7.0 software against the observed experimental patterns. **2D-F-PPV2** reveals AA (eclipsed) stacking with unit cell parameters of $a = 37.4$ Å, $b = 37.4$ Å, $c = 3.5$ Å, $\alpha = 90.0°$, $\beta = 90.0°$, $\gamma = 60°$ with agreement factors of $R_{wp} = 3.68\,\%$ and $R_p = 2.58\,\%$.

The difference plot in Figure 3a reveals the consistency of the refined diffraction pattern with the experimental PXRD data. The FTIR spectra (Figure 3c) of **PPV1**, **F-PPV1**, **PPV2**, and **2D-F-PPV2** display characteristic absorptions around 3000–3300 cm^{-1} [aromatic C–H valence vibrations, ν(C–H)] and at around 1595–1602 cm^{-1} [vinylene stretches ν(C=C)]. Vibrations of the triazine core of **PPV2** and **2D-F-PPV2** are visible at 1505 and 1357 cm^{-1}, respectively. Additionally, –CHO end groups at terminal TFPB/TFPT moieties are indicated by weak carbonyl vibrations ν(C=O) at 1680–1703 cm^{-1}. On top of that, the presence of phosphonate end groups [–$CH_2PO(OEt)_2$] is indicated by weak signals at 950–1025 cm^{-1} [ν(P–O–C)]. The ^{13}C-ssNMR (Figure 3d) spectra of **PPV1**, **F-PPV1**, **PPV2**, and **2D-F-PPV2** show signals attributed to the vinylene C (130 ppm) atoms, and the signals of the secondary/tertiary benzene ring C atoms appear at ca. 130 and 140–144 ppm, respectively. The triazine C atoms of the TFPT moieties appear at shifts of 170 ppm (**PPV2**, **2D-F-PPV2**), whereas the tertiary C atoms of the fluorinated moieties (from building block **2**) appear at 114 ppm (**F-PPV1**, **2D-F-PPV2**).

Motivated by the above results, we further investigated the role of the fluorinated phosphonate **2** on the crystallinity and expanded the investigation to other 2D CPs. Therefore, we synthesized the literature-reported **2D-PPQV1**[30] and the new **2D-F-PPQV1** in an A_6B_2-type polycondensation by heating 2,3,8,9,14,15-hexa(4-formylphenyl)diquinoxalino[2,3-*a*:2′,3′-*c*]phenazine (HATN-6CHO, **7**), (fluorinated) phosphonate **1** or **2** and Cs_2CO_3 as a base in a mixture of Mes/DMAc (1:1) in a sealed glass ampule at 150 °C for three days (Figure 4a).

The crystalline layered structure of **2D-F-PPQV1** was revealed by experimental and simulated PXRDs (Figure 4c). **2D-F-PPQV1** reveals its first reflex at $2\theta = 3.6°$, which is attributed

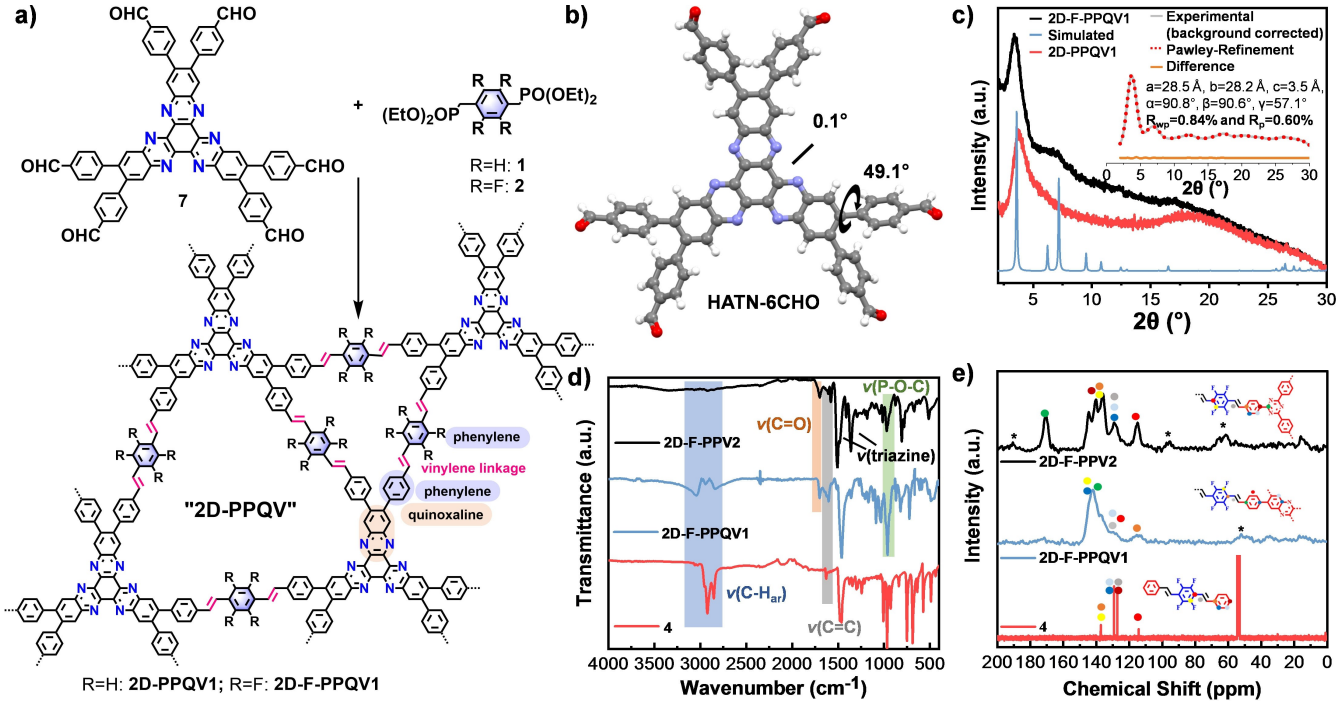

Figure 4. a) Solvothermal synthesis of 2D-poly(phenylene-quinoxaline-vinylene)s (2D-PPQVs) through the Horner-Wadsworth-Emmons polycondensation: phosphonate (**1** or **2**) (59.5 µmol, 3.0 equiv.), HATN-6CHO (**7**) (20.0 mg, 19.8 µmol, 1.0 equiv.) and Cs_2CO_3 (42.6 mg, 130.8 µmol, 6.6 equiv.) were added into a mixture of DMAc (0.45 mL) and Mes (0.45 mL) in a glass ampule. The ampule was sealed under vacuum after three freeze-pump-thaw cycles. After that, the ampule was heated at 150 °C for three days in the oven (**2D-PPQV1**: ca. 75 %, **2D-F-PPQV1**: ca. 74 %). b) Optimized structures (B3LYP 6–31G) of HATN-6CHO (C: gray, N: blue, O: red and H: white). c) PXRD data of **2D-F-PPQV1**: Experimental (black), simulated PXRD with AA layer mismatch (blue) and PXRD data of **2D-PPQV1** (red), as well as the background-corrected PXRD of **2D-F-PPQV1** shown in the inset (background-corrected experimental data (grey), Pawley-Refinement (red), difference plot (orange). d) IR spectra of **2D-F-PPV2**, **2D-F-PPQV1**, and model compound **4**. e) ^{13}C-ssNMR assignment of **2D-F-PPV2**, **2D-F-PPQV1** and ^{13}C NMR of model compound **4** (in DCM-d_2), *sidebands.

to the (110) plane. Besides, a broad reflex at around $2\theta = 5.5°$ to 8.1° appears, assignable to the (210) and (220) planes. The combined (210) and (220) reflex appears only for the fluorinated **2D-F-PPQV1**. Based on the appearance of higher-order reflexes and the slightly lower full-width at half maximum (FWHM) of the first reflex (**2D-PPQV1**: ca. 1.4°, **2D-F-PPQV1**: ca. 1.2°), we identify a superior crystallinity of **2D-F-PPQV1** (see the comparison in Supporting Information, Figure S1), which can be attributed to the combination of HATN-6CHO (**7**) with its planar core (0.11°, Figure 4b) and the employment of electron-poor phosphonate **2**. Experimentally, the formation of crystalline **2D-F-PPQV1** is favored. For **2D-F-PPQV1**, we observed larger cell parameters for the optimized monolayer, AA (eclipsed), AB (staggered), and slipped-AA structures, than those from the experimental PXRD; therefore, a fourth structural motif, where linkers connect obliquely to the next cell (that is, layer one connects to layer two), was optimized (AA mismatch). Optimized interlayer distances, relevant energies, bandgaps, unit cell parameters, HOMO, LUMO, and Fermi level of different stacking modes of **2D-F-PPQV1** can also be found in the Supporting Information. **2D-F-PPQV1** adopts AA layer mismatch stacking with unit cell parameters of $a = 28.5$ Å, $b = 28.2$ Å, $c = 3.50$ Å, $\alpha = 90.8°$, $\beta = 90.6°$, $\gamma = 57.1°$ with agreement factors of $R_{wp} = 0.84\%$ and $R_p = 0.60\%$. The difference plot in Figure 4c shows the consistency of the refined pattern with the experimental PXRD data. Similar to **2D-F-PPV2**, the FTIR spectrum (Figure 4d) of **2D-F-PPQV1** displays characteristic absorptions around 3000–3300 cm^{-1} [aromatic C–H valence vibrations, ν(C–H)], at 1595–1602 cm^{-1} [vinylene stretches ν(C=C)] as well as –CHO end groups [ν(C=O), 1680–1703 cm^{-1}] and phosphonate end groups [(ν(P–O–C), 950–1025 cm^{-1}). Moreover, analogous to **2D-F-PPV2**, the ^{13}C-ssNMR (Figure 4e) spectrum of **2D-F-PPQV1** shows signals of vinylene C (130 ppm) atoms and secondary/tertiary benzene ring C atoms at chemical shifts at ca. 130 and 140–144 ppm, respectively. Furthermore, the 13 C-ssNMR spectra of **2D-F-PPV2** and **2D-FPPQV1** reveal a low-intensity signal matching the presence of $-CH_2PO(OEt)_2$ end groups (ca. 15 and 35 ppm).

Nitrogen physisorption analysis at 77 K revealed the permanent porosity and pore size distribution of the layered crystalline **2D-F-PPV2** and **2D-F-PPQV1**. The Brunauer-Emmett-Teller (BET) surface area was 290 and 186 m^2/g, respectively (Supporting Information, Figure S3). In both cases, the isotherm shows a rise in the low-pressure range ($P/P_o = 0$–0.05), typical for type-I nitrogen sorption. Trapped oligomers and structural defects might explain the moderate BET surface areas. Additionally, a type H4 low-pressure hysteresis can be found in both cases, which can be associated with the deformation of nonrigid pores' walls.[39] Density functional theory was used to determine the pore size distributions, revealing a pore size of approximately 18 Å to 29 Å (1.8–2.9 nm) for **2D-F-PPV2**, which is smaller than the theoretical value (ca. 3 nm). **2D-F-PPQV1** shows a dual-pore distribution with approximately 1.0 Å and 1.9 Å (1.0–1.9 nm), matching well with the theoretical values (ca. 1.0 and 1.7 nm) and the reported values of **2D-PPQV1**.[30] The layered morphology of the synthesized 2D CPs was revealed by high-resolution transmission electron microscopy (HR-TEM) and additionally scanning electron microscopy (SEM) characterizations (Supporting Information, Figure S12).

Next, the optoelectronic properties of the PPVs **PPV1**, **F-PPV1**, **PPV2**, and **2D-F-PPV2** were investigated by UV-Vis absorption and fluorescence spectroscopies (dispersion in 2-propanol). The UV-Vis spectrum (Figure 5a) shows the absorption edge at 463, 473, 490, and 485 nm, respectively. The measured absorption edges correspond to optical band gaps of 2.8, 2.8, 2.6, and 2.6 eV, respectively (Tauc plots in Supporting Information, Figure S5). The fluorescence spectrum (Figure 5b) exhibits an emission maximum at 485, 510, 507, and 538 nm for **PPV1**, **F-PPV1**, **PPV2**, and **2D-F-PPV2**, respectively. Interestingly, the emissions of the fluorinated PPVs (**F-PPV1** and **2D-F-PPV**) show a bathochromic shift of up to 30 nm compared to their non-fluorinated counterparts (**PPV1** and **PPV2**). The PPQVs **2D-F-PPQV1** and **2D-PPQV1** show absorption edges at 552 and 598 nm[30] (E_g ca. 2.3 and 2.2 eV, Tauc plots in Supporting Information, Figure S4), respectively (Figure 5c), while the fluorescence spectra show maxima at 583 and 627 nm[30], respectively. Surprisingly, for the 2D-PPQVs, we do not observe an enlarged Stokes shift for the fluorinated 2D CP, possibly due to the lower influence of the fluorinated moieties on the overall optoelectronic properties.

Moreover, in contrast to the UV-Vis absorption in 2-propanol and 10 M NaOH, the absorption spectra of **2D-F-PPV2** in 10 M HCl demonstrated a bathochromic shift to absorption edges around 600 nm (Figure 5d and UV-Vis in Supporting Information, Figure S8). This shift can be explained by a lack of charge separation due to the resulting cationic resonance structures.[30]

The chemical stability of **2D-F-PPV2** and **2D-F-PPQV1** was investigated by immersing them into sodium hydroxide solution (10 M $NaOH_{aq}$) or hydrochloric acid (10 M HCl_{aq}) for

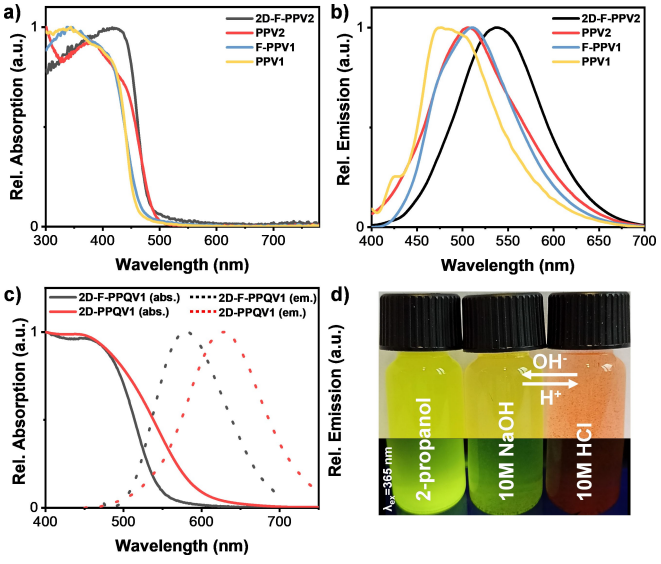

Figure 5. a) UV-Vis absorption and b) fluorescence spectra ($\lambda_{ex} = 375$ nm) of **PPV1** (yellow), **F-PPV1** (blue) **PPV2** (red) and **2D-F-PPV2** (black) (dispersions in 2-propanol). c) UV-Vis absorption (solid lines) and fluorescence spectra (dashed lines, $\lambda_{ex} = 400$ nm) of **2D-F-PPQV1** (black) and **2D-PPQV1** (red) (dispersions in 2-propanol). Photographs of c) **2D-F-PPV2** dispersions in 2-propanol, 10 M NaOH, and 10 M HCl.

three days, respectively. PXRD and IR spectra of **2D-F-PPV2** and **2D-F-PPQV1** proved their unchanged crystallinity and chemical identity (Supporting Information, Figure S7). Moreover, thermogravimetric analysis (TGA) of **2D-F-PPV2** and **2D-F-PPQV1** reveals good thermal stability up to 400 °C (Supporting Information, Figure S9).

Conclusion

In summary, we demonstrated the crystallinity control of novel vinylene-linked 2D CPs using the HWE polycondensation by rational monomer design. Experimentally, we conclude that using rigid and planar building blocks compensates a poor reversibility and error correction. Besides, our experiments show that electron-poor fluorinated phosphonates can increase the crystallinity of the HWE reaction. Those findings are supported by DFT calculations indicating a higher energy barrier for the fluorinated phosphonates, possibly increasing the reversibility of the C–C single bond formation. The structures of the layered 2D CPs were elucidated by PXRD, nitrogen physisorption measurements, IR, ^{13}C-ssNMR, etc, providing insights into the nature of the novel crystalline and porous **2D-F-PPV2** and **2D-F-PPQV1**. Interestingly, the fluorescence spectra of the fluorinated PPVs (**F-PPV1** and **2D-F-PPV**) showed a bathochromic shift of up to 30 nm compared to their non-fluorinated counterparts (**PPV1** and **PPV2**), while the fluorinated **2D-F-PPQV1** shows a hypsochromic shift of ca. 44 nm in comparison to non-fluorinated **2D-PPQV1**. This work thus contributes to the in-depth understanding of the HWE polycondensation to enable the development of unprecedented vinylene-linked 2D CPs with enhanced crystallinity and novel functions.

Acknowledgements

This research was supported financially by the Graphene Flagship Core 3, the Collaborative Research Centre (CRC) 1415 "Chemistry of Synthetic Two-Dimensional Materials" (No. 417590517), H2020-MSCA-ITN (ULTIMATE, No. 813036), the Center for Advancing Electronics Dresden (cfaed), the ERC Consolidator Grant "T2DCP", and the Coordination Networks: Building Blocks for Functional Systems (SPP 1928, COORNET). We thank M. Sc. Lukas Sporrer for SEM measurements, Dr. Kejun Liu for TEM measurements, M. Sc. Tobias Nickel for PXRD and NMR measurements, Dr. Valeriya Tkachova for mass spectroscopy, Matthias Kluge for TGA measurements. We also acknowledge B. Sc. Max Klotzsche and M. Sc. Cindy Rau for practical support as a student research assistant. Furthermore, we recognize using the facilities in the Dresden Center for Nanoanalysis (DCN) at the Technische Universität Dresden. Computational resources were provided by the Center for Information Services and High-Performance Computing (ZIH) of the Technische Universität Dresden. Furthermore, MAA thanks the Materials Chemistry Consortium for HPC time on Young EP/T022213. Open Access funding enabled and organized by Projekt DEAL.

Conflict of Interest

The authors declare no conflict of interest.

Data Availability Statement

The data that support the findings of this study are available in the supplementary material of this article.

Keywords: 2D covalent organic frameworks (2D COFs) · 2D conjugated polymers · Horner-Wadsworth-Emmons reaction · sp^2 carbon-conjugated · vinylene- linked

[1] A. Moliton, R. C. Hiorns, *Polym. Int.* **2004**, *53*, 1397–1412.
[2] K. S. Novoselov, A. K. Geim, S. V. Morozov, D. Jiang, Y. Zhang, S. V. Dubonos, I. V. Grigorieva, A. A. Firsov, *Science* **2004**, *306*, 666–669.
[3] K. S. Novoselov, A. K. Geim, S. V. Morozov, D. Jiang, M. I. Katsnelson, I. V. Grigorieva, S. V. Dubonos, A. A. Firsov, *Nature* **2005**, *438*, 197–200.
[4] A. H. Castro Neto, F. Guinea, N. M. R. Peres, K. S. Novoselov, A. K. Geim, *Rev. Mod. Phys.* **2009**, *81*, 109–162.
[5] S. Wan, F. Gándara, A. Asano, H. Furukawa, A. Saeki, S. K. Dey, L. Liao, M. W. Ambrogio, Y. Y. Botros, X. Duan, S. Seki, J. F. Stoddart, O. M. Yaghi, *Chem. Mater.* **2011**, *23*, 4094–4097.
[6] S. Kandambeth, A. Mallick, B. Lukose, M. V. Mane, T. Heine, R. Banerjee, *J. Am. Chem. Soc.* **2012**, *134*, 19524–19527.
[7] X. Chen, M. Addicoat, S. Irle, A. Nagai, D. Jiang, *J. Am. Chem. Soc.* **2013**, *135*, 546–549.
[8] L. Ascherl, T. Sick, J. T. Margraf, S. H. Lapidus, M. Calik, C. Hettstedt, K. Karaghiosoff, M. Döblinger, T. Clark, K. W. Chapman, F. Auras, T. Bein, *Nat. Chem.* **2016**, *8*, 310–316.
[9] S. Xu, M. Richter, X. Feng, *Acc. Mater. Res.* **2021**, *2*, 252–265.
[10] X. Zhuang, W. Zhao, F. Zhang, Y. Cao, F. Liu, S. Bi, X. Feng, *Polym. Chem.* **2016**, *7*, 4176–4181.
[11] R. Gutzler, D. F. Perepichka, *J. Am. Chem. Soc.* **2013**, *135*, 16585–16594.
[12] A. P. Côté, A. I. Benin, N. W. Ockwig, M. O'Keeffe, A. J. Matzger, O. M. Yaghi, *Science* **2005**, *310*, 1166–1170.
[13] J. Guo, Y. Xu, S. Jin, L. Chen, T. Kaji, Y. Honsho, M. A. Addicoat, J. Kim, A. Saeki, H. Ihee, S. Seki, S. Irle, M. Hiramoto, J. Gao, D. Jiang, *Nat. Commun.* **2013**, *4*, 2736.
[14] T. Banerjee, F. Haase, S. Trenker, B. P. Biswal, G. Savasci, V. Duppel, I. Moudrakovski, C. Ochsenfeld, B. V. Lotsch, *Nat. Commun.* **2019**, *10*, 1–10.
[15] Z. Li, N. Huang, K. H. Lee, Y. Feng, S. Tao, Q. Jiang, Y. Nagao, S. Irle, D. Jiang, *J. Am. Chem. Soc.* **2018**, *140*, 12374–12377.
[16] E. Jin, M. Asada, Q. Xu, S. Dalapati, M. A. Addicoat, M. A. Brady, H. Xu, T. Nakamura, T. Heine, Q. Chen, D. Jiang, *Science* **2017**, *357*, 673–676.
[17] E. Jin, J. Li, K. Geng, Q. Jiang, H. Xu, Q. Xu, D. Jiang, *Nat. Commun.* **2018**, *9*, 4143.
[18] S. Xu, Y. Li, B. P. Biswal, M. A. Addicoat, S. Paasch, P. Imbrasas, S. W. Park, H. Shi, E. Brunner, M. Richter, S. Lenk, S. Reineke, X. Feng, *Chem. Mater.* **2020**, *32*, 7985–7991.
[19] Y. Zhao, H. Liu, C. Wu, Z. Zhang, Q. Pan, F. Hu, R. Wang, P. Li, X. Huang, Z. Li, *Angew. Chem. Int. Ed.* **2019**, *58*, 5376–5381; *Angew. Chem.* **2019**, *131*, 5430–5435.
[20] H. Lyu, C. S. Diercks, C. Zhu, O. M. Yaghi, *J. Am. Chem. Soc.* **2019**, *141*, 6848–6852.
[21] M. Tian, Y. Wang, X. Bu, Y. Wang, X. Yang, *Catal. Sci. Technol.* **2021**, *11*, 4272–4279.
[22] W. R. Cui, C. R. Zhang, W. Jiang, F. F. Li, R. P. Liang, J. Liu, J. D. Qiu, *Nat. Commun.* **2020**, *11*, 1–10.
[23] S. Xu, G. Wang, B. P. Biswal, M. Addicoat, S. Paasch, W. Sheng, X. Zhuang, E. Brunner, T. Heine, R. Berger, X. Feng, *Angew. Chem. Int. Ed.* **2019**, *58*, 849–853; *Angew. Chem.* **2019**, *131*, 859–863.
[24] J. Xu, Y. He, S. Bi, M. Wang, P. Yang, D. Wu, J. Wang, F. Zhang, *Angew. Chem. Int. Ed.* **2019**, *58*, 12065–12069; *Angew. Chem.* **2019**, *131*, 12193–12197.
[25] S. Xu, H. Sun, M. Addicoat, B. P. Biswal, F. He, S. Park, S. Paasch, T. Zhang, W. Sheng, E. Brunner, Y. Hou, M. Richter, X. Feng, *Adv. Mater.* **2021**, *33*, 2006274.

[26] S. Wei, W. Zhang, P. Qiang, K. Yu, X. Fu, D. Wu, S. Bi, F. Zhang, *J. Am. Chem. Soc.* **2019**, *141*, 14272–14279.
[27] D. Becker, B. P. Biswal, P. Kaleńczuk, N. Chandrasekhar, L. Giebeler, M. Addicoat, S. Paasch, E. Brunner, K. Leo, A. Dianat, G. Cuniberti, R. Berger, X. Feng, *Chem. A Eur. J.* **2019**, *25*, 6562–6568.
[28] A. Acharjya, P. Pachfule, J. Roeser, F. Schmitt, A. Thomas, *Angew. Chem. Int. Ed.* **2019**, *58*, 14865–14870; *Angew. Chem.* **2019**, *131*, 15007–15012.
[29] T. Jadhav, Y. Fang, W. Patterson, C. Liu, E. Hamzehpoor, D. F. Perepichka, *Angew. Chem. Int. Ed.* **2019**, *58*, 13753–13757; *Angew. Chem.* **2019**, *131*, 13891–13895.
[30] D. L. Pastoetter, S. Xu, M. Borrelli, M. Addicoat, B. P. Biswal, S. Paasch, A. Dianat, H. Thomas, R. Berger, S. Reineke, E. Brunner, G. Cuniberti, M. Richter, X. Feng, *Angew. Chem. Int. Ed.* **2020**, *59*, 23620–23625; *Angew. Chem.* **2020**, *132*, 23827–23832.
[31] K. László, C. Barbara, "Strategic Applications of Named Reactions in Organic Synthesis, 1st Edition | ISBN 9780124297852," **2005**.
[32] A. P. Davey, A. Drury, S. Maier, H. J. Byrne, W. J. Blau, *Synth. Met.* **1999**, *103*, 2478–2479.
[33] Y. Morisaki, H. Chen, Y. Chujo, *Polym. Bull.* **2003**, *50*, 39–46.
[34] P. Shen, G. Sang, J. Lu, B. Zhao, M. Wan, Y. Zou, Y. Li, S. Tan, *Macromolecules* **2008**, *41*, 5716–5722.
[35] K. Tajima, Y. Suzuki, K. Hashimoto, *J. Phys. Chem. C* **2008**, *112*, 8507–8510.
[36] Z. A. Page, Y. Liu, E. Puodziukynaite, T. P. Russell, T. Emrick, *Macromolecules* **2016**, *49*, 2526–2532.
[37] B. Aradi, B. Hourahine, T. Frauenheim, *J. Phys. Chem. A* **2007**, 5678–5684.
[38] M. Elstner, D. Porezag, G. Jungnickel, J. Elsner, M. Haugk, T. Frauenheim, *Phys. Rev. B: Condens. Matter Mater. Phys.* **1998**, *58*, 7260–7268.
[39] S. Yurdakal, C. Garlisi, L. Özcan, M. Bellardita, G. Palmisano, *Heterog. Photocatal. Relationships with Heterog. Catal. Perspect.* **2019**, 87–152.

Manuscript received: December 18, 2021
Accepted manuscript online: February 14, 2022
Version of record online: March 11, 2022